Influence of Shear Stiffness of Geocell Mattress on the Performance of Strip Footings: A Numerical Study

P. A. Faby Mole[1], S. Sireesh[2*] and M. R. Madhav[3]
[1]*Former Master's Student, Department of Civil Engineering, Indian Institution of Technology Hyderabad, India*
[2]*Associate Professor, Department of Civil Engineering, Indian Institution of Technology Hyderabad, India*
[3]*Visiting Professor, Department of Civil Engineering, Indian Institution of Technology Hyderabad, India*
[2*]*Corresponding Author, E-mail*: sireesh@iith.ac.in

ABSTRACT: A modified Pasternak model was proposed to predict the behavior of a strip footing resting on a geocell reinforced granular layer overlying weak soil, especially considering the variation of shear stiffness of the geocell mattress. Both linear and nonlinear responses of the geocell reinforced beds were considered in the analysis. Results from the present model were validated with independent experimental load-deformation responses. The model parameters viz. inverse of normalized shear stiffness of the geocell and inverse of normalized ultimate bearing capacity of foundation soil were varied for the parametric study. It was found that the shear stiffness of the reinforced granular bed i.e. the product of shear modulus and the height of the geocell reinforced granular bed plays an important role in improving the performance of the foundation system. Design charts are presented in the form of improvement factors for the practical range of shear layer width, shear stiffness of the geocell reinforcement and ultimate bearing capacity of the soft soil.

KEYWORDS: Strip footing, Geocell reinforcement, Shear stiffness, Soft soil

1. INTRODUCTION AND BACKGROUND

Widespread research on the use of geocells, which provide all-round confinement to the infill material, as a foundation soil reinforcement, has been carried out by various researchers (Bathurst and Jerrett, 1989, Cowland and Wong, 1993). The cellular confinement system was first developed and evaluated in France during late 1970s (Koerner, 1990). Since then, the use of geocells in the construction industry has gained wide spread popularity due to its advantages over the two-dimensional planar form of geosynthetics. Geosynthetics rely on frictional resistance, arching, and entanglement of fibers to improve the soil performance, whereas, geocell derives its strength from the all-round confinement, the three-dimensional geocell mattress offers to the encapsulated soil along with friction.

Many research studies have proposed models for understanding the response of geosynthetic reinforced foundations. Madhav et al. (1988) proposed an improved Pasternak model (1954) that incorporates a rough membrane to simulate the behavior of geosynthetic reinforcement in the foundation system. They further developed the model (Madhav et al. 1989) to incorporate the lateral restraint effect of the geosynthetics. Later, the settlement response of the planar geosynthetic reinforced granular fill soft soil system was predicted by a mechanical foundation model (Shukla and Chandra, 1994). Deb et al. (2007) proposed a similar model to predict the behavior of a geogrid reinforced granular fill over soft soil stabilized with stone columns to reduce total and differential settlements.

In all the above models, the geosynthetic layer was modeled as a membrane subjected to tension. However, modeling the behavior of a three-dimensional geocell mattress with infill material is a complex task. Authors have attempted to model the behavior of geocell reinforcement under strip footing (Faby Mole et al. 2015). However, the stress dependency of the geocell mattress, which varies from the center of the footing to the edge of the mattress was not considered in their earlier model.

In this study, an attempt has been made to consider the stress dependent behavior of geocell mattress in supporting the rigid strip footing over weak foundation soils.

2. PROBLEM DEFINITION

The present approach improves the previous model discussed in Faby Mole et al. (2015) by incorporating the confinement effect of the geocell reinforced ground. The major shortcoming in the model discussed earlier is that it do not account for the variation in shear modulus of the geocell layer from the center to the edge of the geocell layer. The present study explains the behavior of geocell reinforced granular layer (associated stress dependency) over soft soil under rigid strip footing as shown in Figure 1.

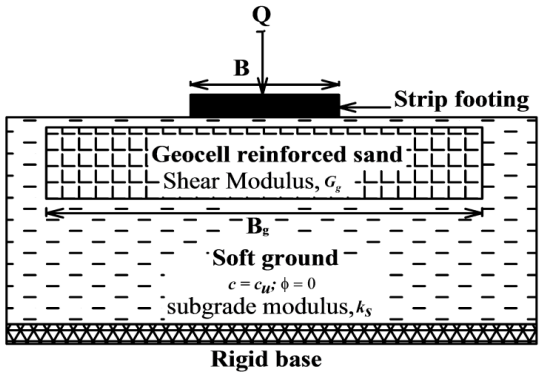

Figure 1 Definition sketch of strip footing on geocell reinforced foundation bed

A two-parameter elastic model approach was adopted to idealize the proposed model (Figure 2a). The corresponding deflection profile as per Pasternak model is shown in Figure 2b. Since rigid footing is considered, the settlement under the loaded strip footing is uniform and the pattern varies from the edge of the footing to the edge of the geocell as described by Pasternak's Equation. The linear and nonlinear response models were analyzed for low and high settlements, respectively. Soil - Geocell properties were varied to obtain optimized improvement of the soft ground.

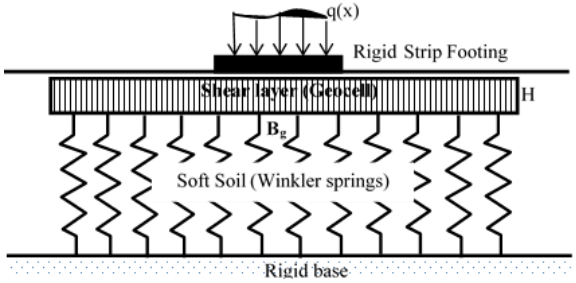

Figure 2a Idealized Pasternak shear layer over Winkler springs

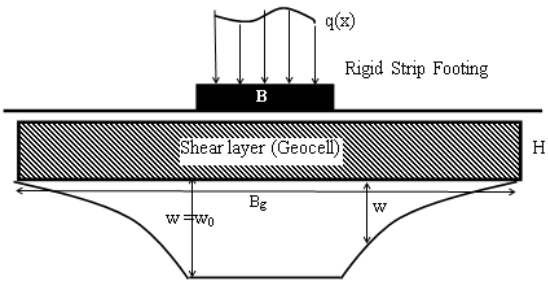

Figure 2b Deflection profile of Pasternak shear layer over Winkler springs

3. MATHEMATICAL FORMULATION

3.1 Linear Formulation

The governing equation for the load-deflection pattern of the problem (Figure 2b), with the aid of Pasternak model incorporating the stress dependent behavior is presented below:

$$q(x) = k_s.w_o \quad \text{for} \quad 0 \le |x| \le \frac{B}{2} \tag{1}$$

$$k_s.w - G_g.H.\frac{d^2w}{dx^2} = 0 \quad \text{for} \quad \frac{B}{2} \le |x| \le \frac{B_g}{2} \tag{2}$$

To represent the terms in non-dimensional form, let

$$X = \frac{x}{B}, \quad W = \frac{w}{B}$$

Simplifying Eq. (2), the governing equation reduces to

$$\frac{d^2W}{dX^2} - \alpha^2 W = 0 \tag{3}$$

Where,

$$\alpha^2 = \left(\frac{k_s.B^2}{G_g.H}\right)$$

Where, α is inverse of normalized shear stiffness of geocell reinforced soil; k_s is subgrade modulus; B is the width of the strip footing; G_g is the shear modulus of shear layer; B_g and H are the width and height of the shear layer, respectively.

Equation (3) represents the deflection profile of the foundation system from the edge of the footing to the edge of the geocell. It is well established that the modulus of deformation or the shear modulus of the soil is directly proportional to the confining stress. As per Janbu's relation, the shear modulus is a function of confining stress as shown:

$$G = G_0\left(\frac{\sigma'}{\sigma_0'}\right)^n \tag{4}$$

Where, G is shear modulus of the soil; G_0 is initial shear modulus of the soil; σ' and σ'_0 are the present and initial confining stresses; and n is Janbu's stress exponent number. Generally, n values ranges between 0 and 1. The Janbu's stress exponent, $n = 1$ is used for over-consolidated clays to represent a constant modulus and $n = 0$ to represent linearly varying modulus (Janbu, 1963).

Now, consider an elemental area in the shear layer along with the acting on as shown in Figure 3.

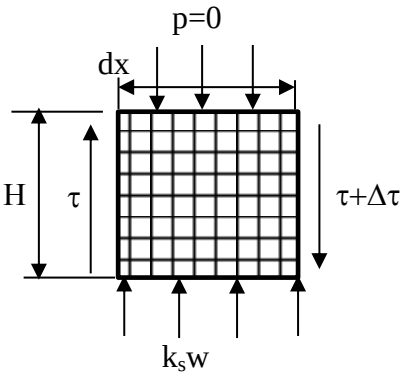

Figure 3 Forces acting on an elemental area

Equate the forces in vertical direction (Figure 3) by assuming the downward forces acting on the element to be zero, as the weight of the infinitesimal element is negligible, yields:

$$(k_s w)dx + \tau H - (\tau + \Delta\tau)H = 0 \tag{5}$$

Dividing throughout the Eq. (5) by dx, one gets

$$k_s w - \frac{\Delta\tau}{dx}H = 0 \tag{6}$$

The shear stress is expressed in terms of shear strain as

$$\tau = G\frac{dw}{dx} \tag{7}$$

Differentiating Eq. (7),

$$\frac{\Delta\tau}{dX} = G\frac{d^2w}{dx^2} + \frac{dw}{dx}\frac{dG}{dx} \tag{8}$$

$$\frac{dG}{dx} = \frac{G_0}{(\sigma_0')^n}n(\sigma_0' + \Delta\sigma')^{n-1}\frac{d\Delta\sigma'}{dx} \tag{9}$$

Let us assume the incremental stress, $\Delta\sigma' = (k_s w)/2$ (i.e. the average of upward and downward stresses).
Let us represent the initial stress as

$$\sigma_0' = Ck_sB \tag{10}$$

Substituting, Eq. (8) and Eq. (10) in Eq. (6)

$$k_s w - G_0\left(\frac{\sigma'}{\sigma_0'}\right)^n H\frac{d^2w}{dx^2} - \frac{dw}{dx}\frac{G_0}{(\sigma_0')^n}n(\sigma_0' + \Delta\sigma')^{n-1}\frac{d\Delta\sigma'}{dx}H = 0 \tag{11}$$

Expressing the eqn. in non-dimensional form
Let $W=w/B$, $X=x/B$,

$$\left(\frac{C+\frac{W}{2}}{C}\right)^{n}\frac{d^2W}{dX^2}+\frac{1}{2}\left(\frac{dW}{dX}\right)^2\frac{1}{C^n}n\left(C+\frac{W}{2}\right)^{n-1}-\alpha^2W=0 \tag{12}$$

Where,

$$\alpha^2=\frac{k_sB^2}{G_0H}$$

Equation (12) represents the deflection profile from the edge of the footing to the edge of the geocell layer taking the geocell properties (α) and compaction coefficient (C) into account. The parameter, n is assumed as 0.5 in the present analysis for silty sandy soils (Janbu, 1963).

The load deflection of the formulation is as follows:

$$q(x).B=Q=k_sBw_0+2\int_{B/2}^{B_{g/2}}k_s w\,dx \tag{13}$$

Dividing Eq. (13) with (k_sB^2) yields

$$Q^*=W_0+2\int_{0.5}^{R_{g/2}}W dX \tag{14}$$

3.1.1 Validation

Equation (12) is a modification of Eq. (3) incorporating the confinement effect to obtain the deflection profile of rigid strip footing on geocell reinforced soil. Equation (12) reduces to Eq. (3) when n = 0. The stress-dependent model was validated against the theoretical solution given by Faby et al. (2015) for stress independent model, and the results are found in very good agreement with each other as the set of curves coincided with each other as shown in Figure 4.

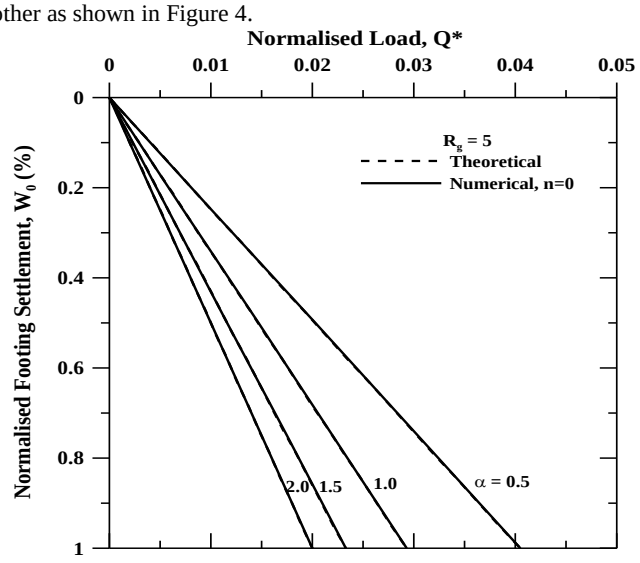

Figure 4 Comparison of numerical (after linearization) and theoretical results

3.1.2 Discussion

The deflection profiles from the edge of the footing to the edge of the geocell are shown in Figure 5. The solid lines represent the model that predicts the settlement pattern near to the actual behavior incorporating the confining stresses in the geocell layer. In the stress independent analysis, the shear modulus of the geocell is taken as constant throughout the shear layer, whereas the improved model considers the variation in shear modulus of the geocell layer. The improved model shows a uniform distribution of load with high bearing capacity.

The corresponding load-settlement with variation in geocell layer stiffness (α) is presented in Figure 6. As expected, the model incorporating the confining effect/stress dependency is able to withstand higher loads. The previous model under predicts the actual behavior. The linear load-settlement curve is applicable for very low normalized settlements of the order of 1%.

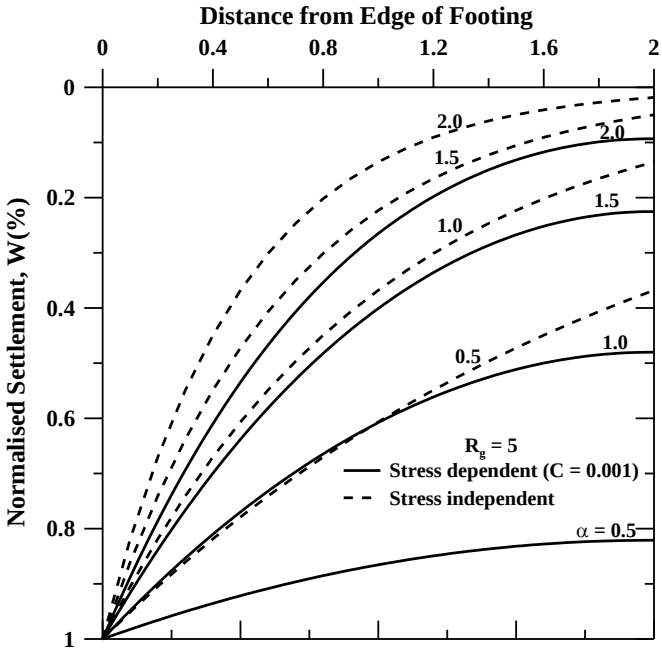

Figure 5 Settlement Profile from the edge of the footing to the edge of the geocell layer

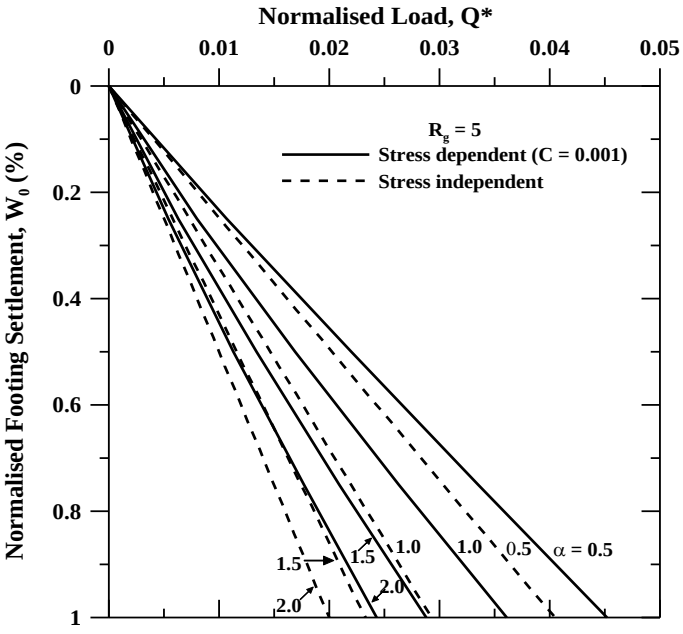

Figure 6 Linear load-settlement curve (Variation in α)

3.2 Nonlinear formulation

The nonlinear stress-displacement response of the soil can be represented by hyperbolic relation presented by Kondner (1963)

$$q(x)=\frac{k_s.w_0}{1+\frac{k_s}{q_u}.w_0} \quad \text{for} \quad 0\le|x|\le\frac{B}{2} \tag{15}$$

$$\frac{k_s.w}{1+\frac{k_s}{q_u}.w}-G_g H\frac{d^2w}{dx^2}=0 \quad \text{for} \quad \frac{B}{2}\le|x|\le\frac{B_g}{2} \tag{16}$$

To represent the terms in non-dimensional form, let

$$X=\frac{x}{B},\quad W=\frac{w}{B}$$

Simplifying Eq. (16), the governing equation reduces to

$$\frac{d^2W}{dX^2}-\alpha^2\frac{W}{1+\mu.W}=0 \tag{17}$$

Where,

$$\alpha^2=\left(\frac{k_s.B^2}{G_g H}\right) \quad \text{and} \quad \mu=\frac{k_s.B}{q_u}$$

Equating the forces in vertical direction,
Assume the downward force acting on the element, p = 0

$$\left(\frac{k_s w}{1+\frac{k_s w}{q_u}}\right)dx+\tau H-(\tau+\Delta\tau)H=0 \tag{18}$$

Dividing Eq. (18) throughout by (dx)

$$\left(\frac{k_s w}{1+\frac{k_s w}{q_u}}\right)-\frac{\Delta\tau}{\partial x}H=0 \tag{19}$$

Substituting for τ from Eq. (7),

$$\left(\frac{k_s w}{1+\frac{k_s w}{q_u}}\right)-G_0\left(\frac{\sigma'}{\sigma_0'}\right)^n H\frac{d^2w}{dx^2}-\frac{dw}{dx}\frac{G_0}{(\sigma_0')^n}n(\sigma_0'+\Delta\sigma')^{n-1}\frac{d\Delta\sigma'}{dx}H=0 \tag{20}$$

In non-dimensional form,

$$\left[\frac{C+\frac{1}{2}\left(\frac{W}{1+\mu W}\right)}{C}\right]^n\frac{d^2W}{dX^2}+\frac{1}{2}\frac{1}{C^n}n\left[C+\frac{1}{2}\frac{W}{1+\mu W}\right]^{n-1}\frac{dW}{dX}\frac{d\left(\frac{W}{1+\mu W}\right)}{dX}-\alpha^2\frac{W}{1+\mu W}=0 \tag{21}$$

Equation (21) represents the settlement profile as a function of compaction coefficient, *C*; inverse of normalized shear stiffness geocell reinforced soil (α), inverse of normalized ultimate bearing capacity of subsoil (μ).

The load - deflection equation is

$$q_f(x).B=Q_f=\frac{k_s B w_0}{1+\frac{k_s w_0}{q_u}}+2\int_{B/2}^{B_g/2}\frac{k_s w}{1+\frac{k_s w}{q_u}}dx \tag{22}$$

On simplification one gets

$$\frac{Q_f}{k_s B^2}=Q^*=\frac{W_0}{1+\mu.W_0}+2\int_{0.5}^{R_g/2}\frac{W}{1+\mu.W}dX \tag{23}$$

3.2.1 Finite Difference Formulation

In this study, linear and nonlinear formulations had to be solved using numerical methods. Finite difference method was employed for obtaining the solution. Central difference scheme (Crank-Nicolson method, 1947) was used for discretizing the terms of second order and forward difference scheme (explicit method) was used for first order terms. The linear governing differential equation was discretized as follows:

$$\left(\frac{C+\frac{W_i}{2}}{C}\right)^n\frac{W_{i+1}-2W_i+W_{i-1}}{(\Delta X)^2}+\frac{1}{2}\left(\frac{W_{i+1}-W_i}{\Delta X}\right)^2\frac{1}{C^n}n\left(C+\frac{W_i}{2}\right)^{n-1}-\alpha^2W_i=0 \tag{24}$$

The equation Eq. (24) has to be linearized, to solve using the iterative Gauss-Seidel method.

Let,

$$h(i)=\left[\frac{C+W_i/2}{C}\right]^n \quad \text{where, } n=0.5 \tag{25}$$

$$h(i)\frac{W_{i+1}-2W_i+W_{i-1}}{(\Delta X)^2}+\frac{1}{2}\left(\frac{W_{i+1}-W_i}{\Delta X}\right)^2\frac{1}{C^n}\frac{n}{h(i)}-\alpha^2W_i=0 \tag{26}$$

The governing differential equation is solved to obtain the deflection pattern and the corresponding load deflection equation is solved.

The nonlinear stress dependent model involved high complexity and had to be linearized twice to arrive at the solution. The stress-dependent model in finite difference form (Central and forward difference scheme) is represented as follows:

$$\left[\frac{C+\frac{1}{2}\left(\frac{W_i}{1+\mu W_i}\right)}{C}\right]^n \frac{W_{i+1}-2W_i+W_{i-1}}{(\Delta X)^2}$$

$$+\frac{1}{2}\frac{1}{C^n}n\left[C+\frac{1}{2}\frac{W_i}{1+\mu W_i}\right]^{n-1}\frac{W_{i+1}-W_i}{\Delta X}\frac{\frac{W_{i+1}}{1+\mu W_{i+1}}-\frac{W_i}{1+\mu W_i}}{\Delta X}-\alpha^2\frac{W_i}{1+\mu W_i}=0 \quad (27)$$

The complexity involved in Eq. (24) can be reduced by linearizing the equation as follows:

$$g(i)=\frac{W_i}{1+\mu W_i} \quad (28)$$

$$h(i)=\left[\frac{C+g(i)/2}{C}\right]^n \text{ Where } n=0.5 \quad (29)$$

The equation can be rewritten in the linearized form as

$$h(i)\frac{W_{i+1}-2W_i+W_{i-1}}{(\Delta X)^2}+\frac{1}{2}\frac{1}{Ch(i)}n\frac{W_{i+1}-W_i}{\Delta X}\frac{\frac{W_{i+1}}{1+\mu W_{i+1}}-\frac{W_i}{1+\mu W_i}}{\Delta X}-g(i)\alpha^2=0 \quad (30)$$

The linearized equation is solved to obtain the deflection pattern and the nonlinear load deflection curves.

3.2.2 Boundary Conditions

The settlement of the rigid strip footing is considered as uniform under the loaded footing area. Hence, the normalized settlement (W) at the edge of the footing is equal to the normalized footing settlement (W_0). The slope of the settlement profile (gradient of the settlement profile, dW/dX) is zero at the edge of the geocell layer, i.e. $R=R_g/2$.

These two boundary conditions have been instrumental in solving both linear and non-linear ordinary differential equations.

In mathematical form these conditions can be written as:

at R = 0.5, $W = W_0$

at $R= R_g/2$, dW/dX = 0

3.2.3 Validation

Numerical Validation

At a very high settlement, the load-settlement curve, Eq. (23) converges to a constant Q^*, obtained from Eq. (31).

$$Q^*=\frac{1}{\mu}+2\int_{0.5}^{\frac{R_g}{2}}\frac{1}{\mu}dx=\frac{1}{\mu}+\frac{2}{\mu}\left(\frac{R_g}{2}-0.5\right) \quad (31)$$

To check the accuracy of the stress-dependent model, a trial was carried out at 75% settlements to determine whether it matches with the result obtained from Eq. (31). For R_g = 5 and μ =50, Eq. (31) yields the solution, Q^* = 0.1. The result obtained from the numerical (MATLAB) analysis is, Q^* = 0.0974. The percentage error is -2.73%, which is due to truncation and round-off errors in the finite difference method.

Theoretical Validation

The model incorporating stress dependency (Eq. (21)) reduces to the nonlinear model (Eq. (17)) when Janbu's parameter, n=0. Similar analysis was carried out on the stress dependent model by substituting n=0 and results of nonlinear and stress dependent model were found to be in good agreement as shown in Figure 7.

Experimental Validation

The efficiency of the current model was reviewed with the help of experimental investigations on strip footing on geocell reinforced sand bed conducted by Moghaddas and Dawson (2010). In their study, geocells were formed by cutting a required size of planar, non-perforated geotextile material and thermo-welded at prescribed locations. A poorly graded sand was used as infill material and subjected to a monotonic loading through a 150mm wide model strip footing. From the experimental data the modulus of subgrade reaction, ultimate bearing capacity, static shear modulus of geocell reinforced layer (obtained from elastic modulus) were determined and the values of inverse of shear modulus of the geocell reinforced soil (α) and the inverse of the ultimate bearing capacity of the subsoil (μ) were calculated.

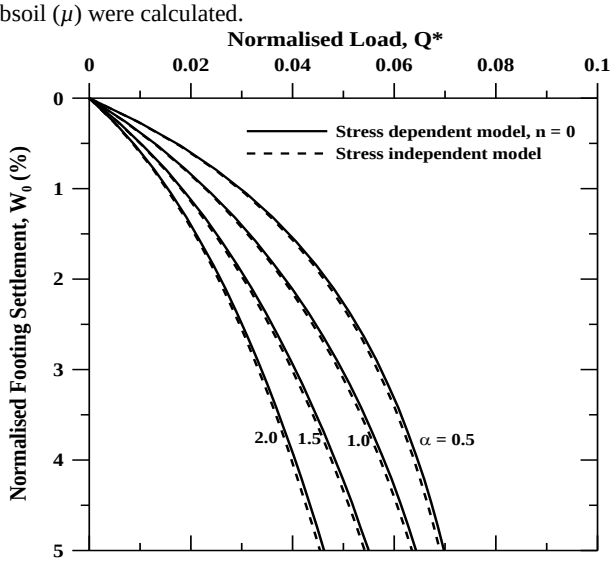

Figure 7 Normalized load-settlement curve – Comparison of stress dependent and nonlinear model

Figure 8 shows the load-settlement curve of the nonlinear stress independent model, stress dependent model and experimental data for the thickness of the geocell reinforced layer (H) is equal to the plate width (B). Thought the validation was performed for other two cases (i.e. H = 0.33B and H = 0.66B) with an acceptable agreement, only the H=B case is presented here. It can be clearly seen that the stress dependent model predicts the experimental data very well up to about 8% of normalized settlement and again at higher settlement range (W_0 = 15 – 20%). The deviation between the experimental and predicted data is due to local strain-hardening behaviour of bed. The prediction of the stress independent model was valid for low normalized settlements of the order of 5% and for higher normalized settlements, stress dependent model predictions are superior. Three cases of the experimental test were analyzed over the complete range of 0-20% normalized settlement, the results are in good agreement.

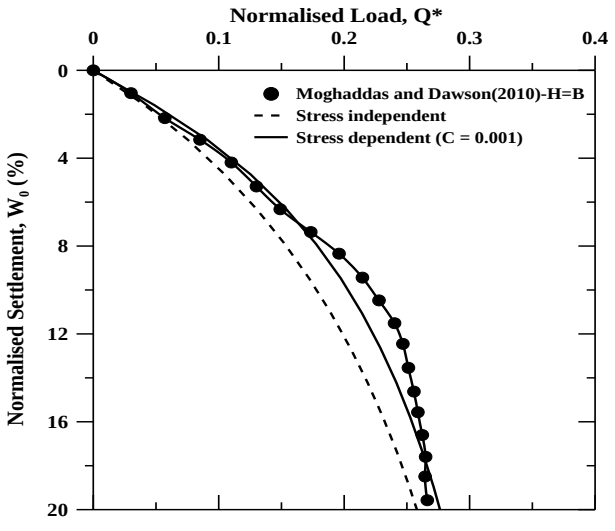

Figure 8 Normalized load-settlement curve – Comparison of the stress dependent and nonlinear model with experimental data

4. RESULTS AND DISCUSSION

The deflection profile from the edge of the footing (*B*) to the edge of the geocell layer (B_g) obtained from the proposed stress dependent model incorporating the nonlinear response are shown in Figure 9. The deflection profiles from stress independent model (Eq. (17)) for different values of α and μ are also plotted as dashed lines in Figure 9. From the figure, it is clear that the stress independent model does not distribute the load uniformly over the weak sub-soil. For geocells with higher shear stiffness, the behavior changes significantly. The corresponding load-settlement pattern is shown in Figure 10 for R_g = 5 and α = 1.0. The load-settlement pattern shows a minimal variation with an increase in geocell layer stiffness (α) when the confinement effect of the geocell is also taken into account. However, similar trends as the stress independent model were observed. The load supported by geocells of higher shear stiffness is high, however, the variation is comparable with that of geocells of lower shear stiffness.

Similarly, the normalized load-settlement patterns for different subsoil conditions (i.e. varying μ) for R_g = 5 and α = 1.0 is presented in Figure 11. The load borne by the geocell reinforced soil is high, especially when the subsoil is of higher strength (μ < 5.0). Besides, for a reasonably stiff geocell mattress (α = 1.0), due to higher confining effect, stress dependent model (C = 0.001) shows a higher load carrying capacity. It can also be seen that the influence of stress dependency is negligible for a very soft foundation soil (μ = 100) for a given geocell mattress stiffness (α = 1.0). As high as 33% and 43% increase in load carrying capacity is observed for stress dependent model at 5% and 10% footing settlements, respectively for the case of μ = 0.

Figure 12 shows the normalized load-settlement curves for various compaction coefficients (C) over the settlement range of 0-20% for various μ and α values. The variation in the load-settlement pattern with stress dependency is significant over the range of 0-10% and converges thereafter to a constant value at higher settlements. The variation in load-settlement curve was found to be maximum for the lower range of μ value ($\mu \leq 50$), i.e. stronger subgrade conditions (Figure 12a). Besides, the influence of confining stress on the load-settlement pattern is negligible for stiffer geocell mattresses ($\alpha \leq 1.0$) (See Figures 12 a, b, c with respect to Fig. 12d). In other words, for a weaker sub soil conditions (μ = 50) the influence of compaction coefficient is considerable for a lower shear stiffness of the geocell mattress (Figure 12d).

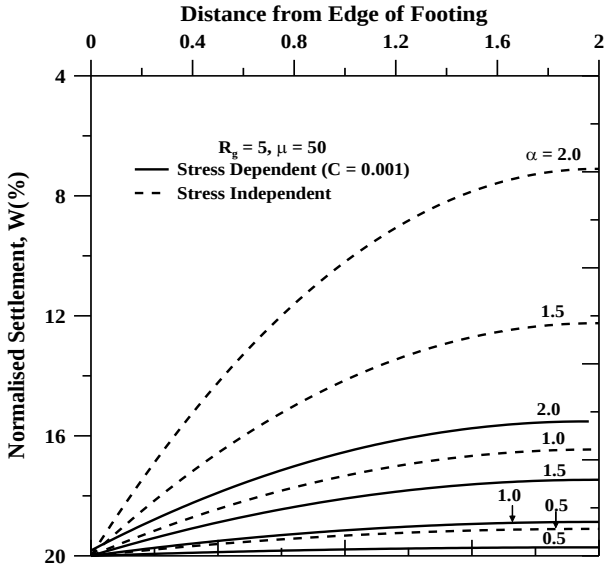

Figure 9 Deflection profiles from the edge of the footing to the edge of the geocell

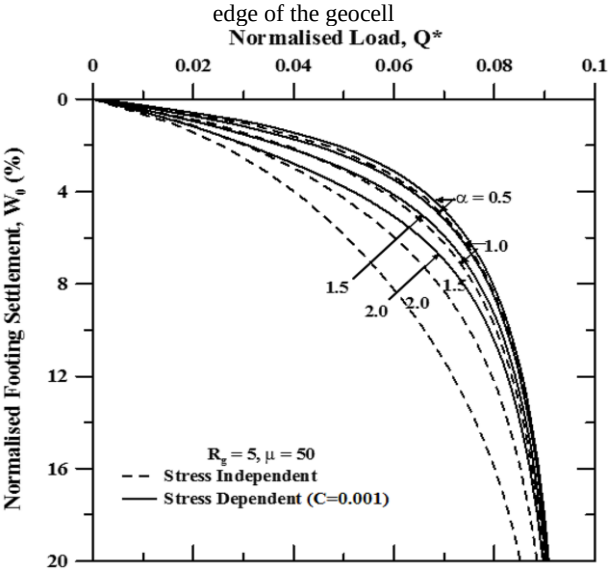

Figure 10 Normalized load-settlement curve (Variation in α)

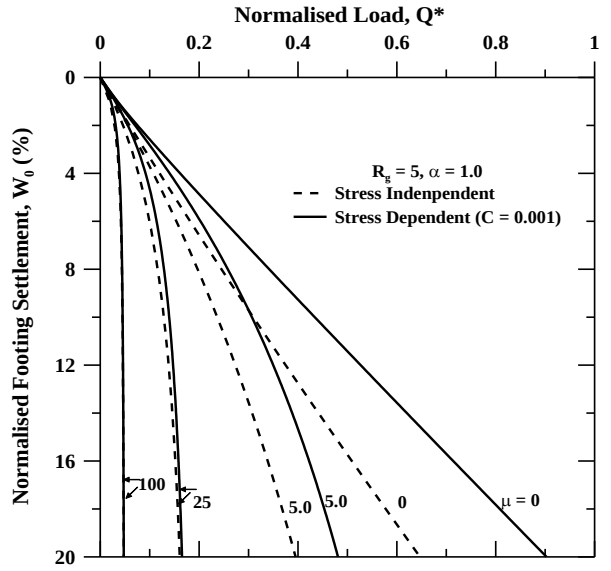

Figure 11 Normalized load-settlement curve (Variation in μ)

The performance improvement of the geocell reinforcement can be further quantified using a non-dimensional factor known as improvement factor (I_f). The improvement factor is defined as a ratio of normalized load (Q*) of reinforced bed to the unreinforced bed for different conditions of the bed (i.e. W, α, μ, R_g *and* C). The variation in improvement factor (I_f) with the inverse of normalized shear stiffness (α) is plotted in Figure 13. Figure 13a shows the variation of I_f with subsoil stiffness it can be inferred from the plot is that for soils of high stiffness (μ=0) the improvement factors are low, because the load-bearing capacity of the soil with high stiffness is very high and hence, further improvement with the inclusion of geocell is marginal. Figure 13b shows the improvement with variation in normalized settlement, and as expected higher improvement is shown at higher settlements. It could also be seen that there is a clear trend of decrease in improvement with low geocell layer stiffness (α = 2), especially for soils with high ultimate bearing capacity and lower range of settlements (3-10%). For a high range of settlements and soils with low stiffness, the improvement remains almost the same with an increase in α.

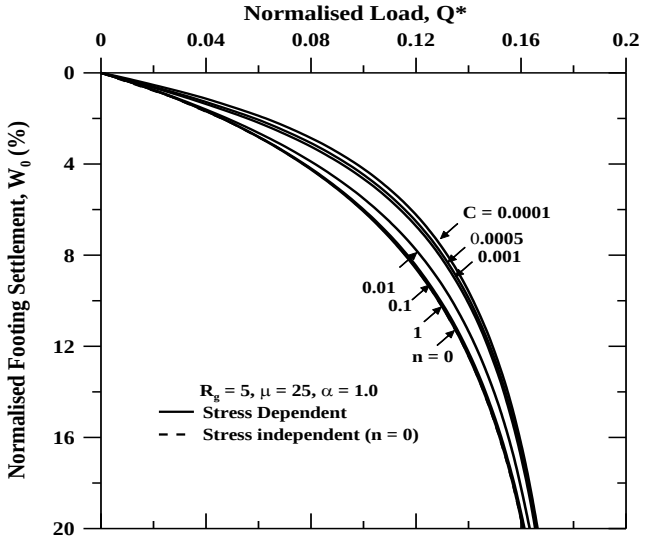

Figure 12a Normalized load-settlement curve for varying C (μ = 25, α= 1)

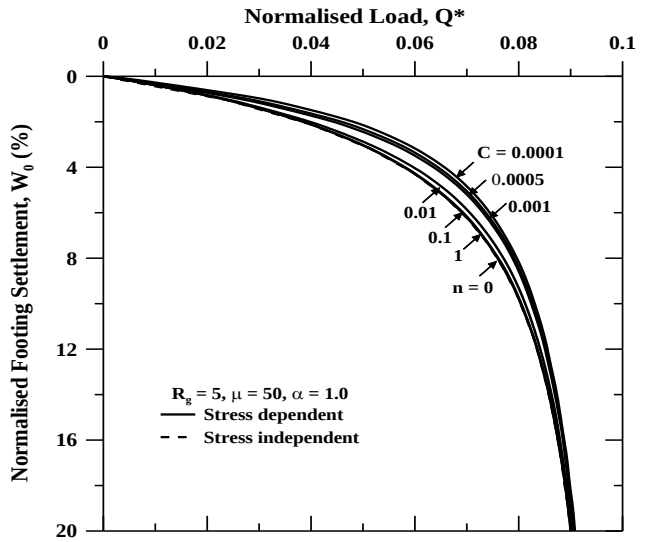

Figure 12b Normalized load-settlement curve for varying C (μ = 50, α = 1)

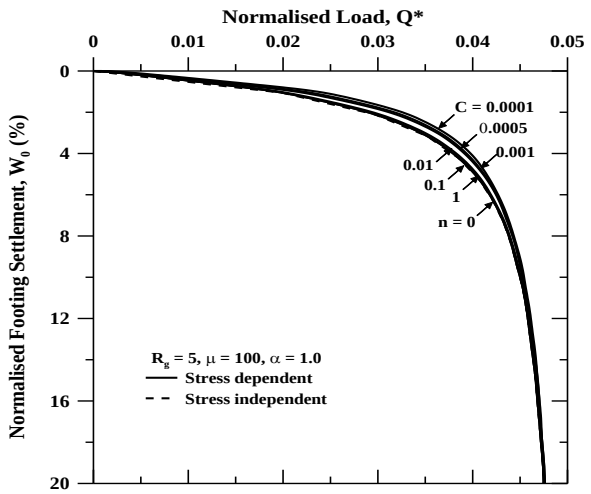

Figure 12c Normalized load-settlement curve for varying C (μ = 100, α = 1)

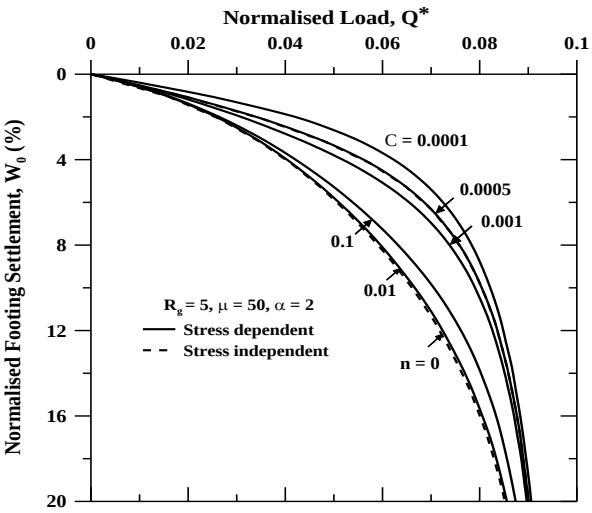

Figure 12d Normalized load-settlement curve for varying C (μ = 50, α = 2)

Figure 12 Normalized load-settlement curve (Variation in C)

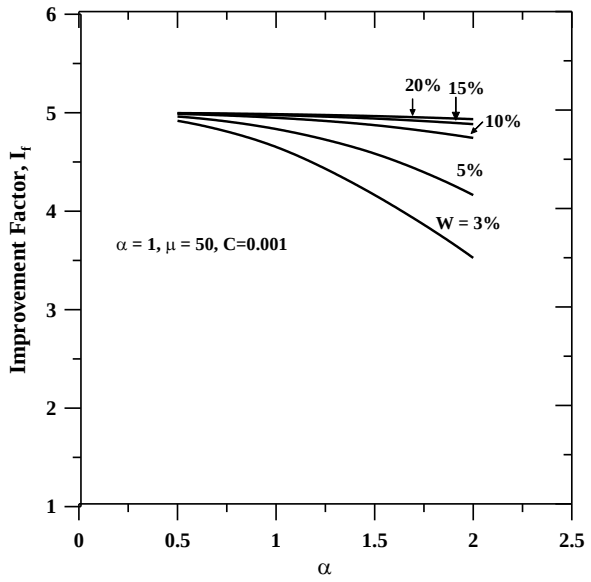

Figure 13a Variation of I_f with α (Varying W_0)

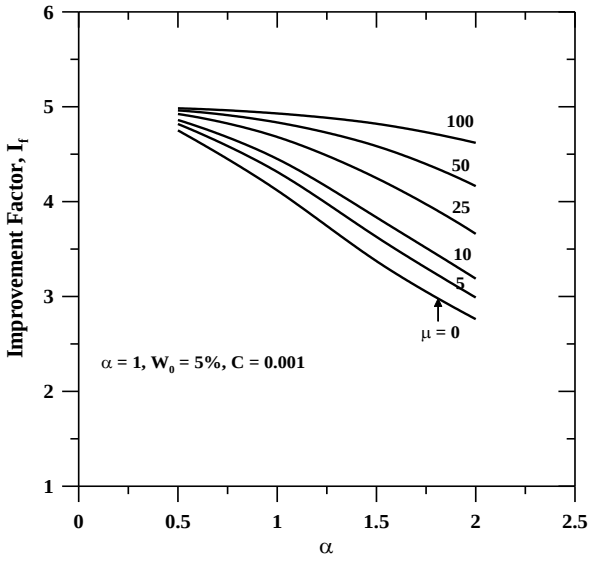

Figure 13b Variation of I_f with α (Varying μ)

Figure 13 Variation of improvement factor (I_f) with inverse of normalized shear stiffness (α)

Figure 14 shows the variation of improvement factor (I_f) with shear layer width ratio (R_g) for different values of μ, C, α, W_0. There is a clear trend of improvement with an increase in geocell layer width but the improvement remains constant beyond R_g= 5 in usual cases. For subsoil of low stiffness, providing R_g beyond 5 also provides a significant improvement (Figure 14a). Similarly, there is a convincing improvement after R_g= 5 for geocell layer of high stiffness, however, improvement is negligible for geocell layers of low stiffness (α=2, Figure 14b). The compaction factor, C that determines the confining stress in the geocells were varied for constant soil-geocell properties and normalized settlement (Figure 14c) and there was a clear trend of improvement with an increase in geocell layer width ratio even up to 10. The improvement factor reported is very high for stress dependent model (Figure 14c). The performance improvement of the soil increase at a constant rate at settlements of the order of 15%, however, for lower settlements of the order of 5%, there is not much further improvement for shear layer width ratio beyond 5.

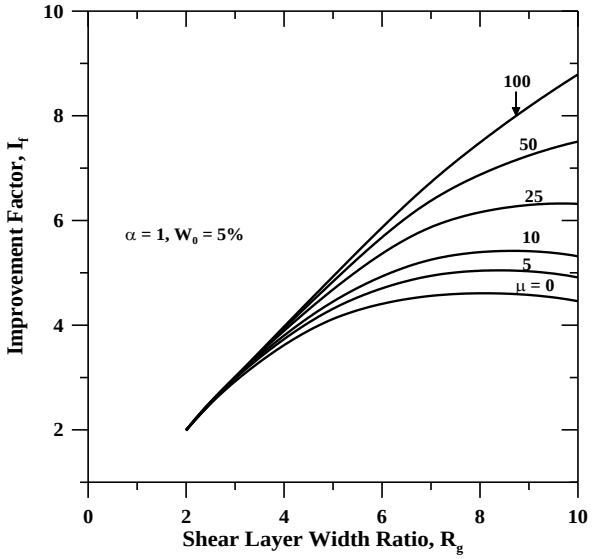

Figure 14a Variation of I_f with R_g (Varying μ)

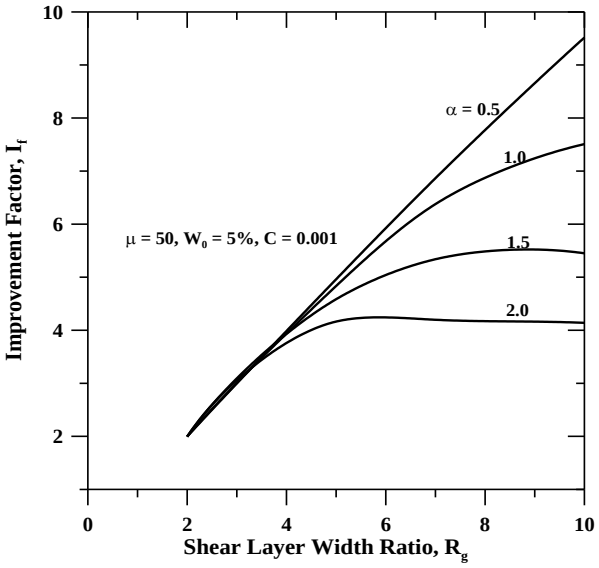

Figure 14b Variation of I_f with R_g (Varying α)

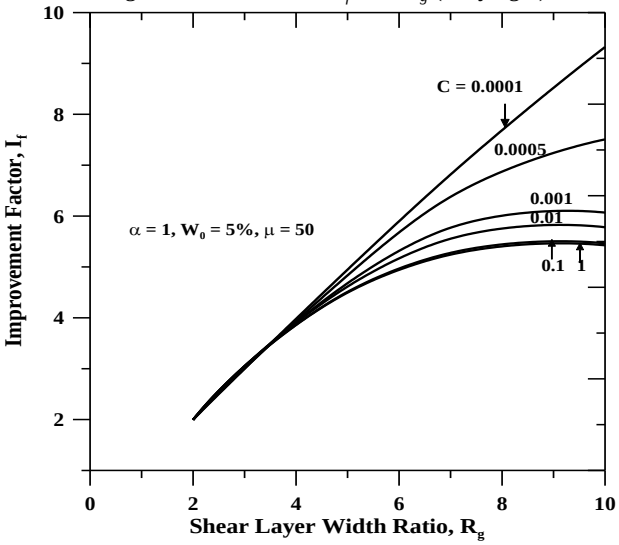

Figure 14c Variation of I_f with R_g (Varying C)

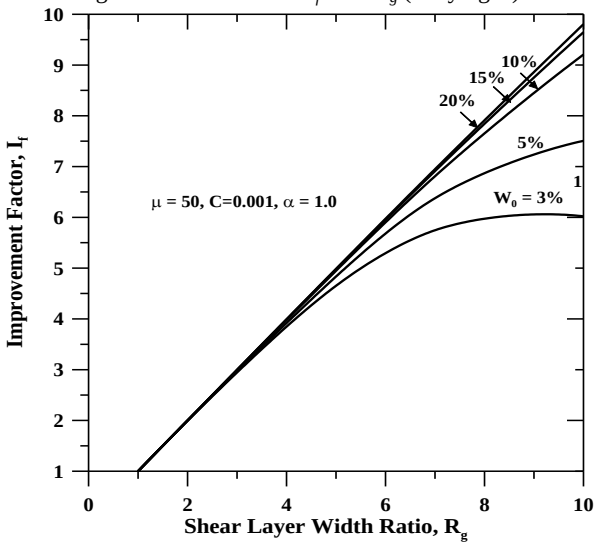

Figure 14d Variation of I_f with R_g (Varying W_0)

Figure 14 Variation of improvement factor (I_f) with shear layer width ratio (R_g)

5. CONCLUSIONS

An attempt has been made to numerically simulate the elasto-plasticbehavior of a rigid strip footing on geocell reinforced bed incorporating the stress dependency of the geocell layer. A modified

Pasternak model was used to obtain the linear and nonlinear responses of the bed. Some of the important observations made from the study are listed below:

The proposed nonlinear stress dependent model was validated with a high accuracy with an independent experimental study. The current model incorporates the actual behavior of geocell which derives its strength from the all-round confinement effect.

The nonlinear stress independent model performed satisfactorily for lower settlement range (s/B < 1%), however, for higher settlements, the model that incorporates stress dependency has to be used.

There is a clear trend of improvement in load carrying capacity with an increase in the shear stiffness of the geocell reinforced ground (α) at low settlement range and high stiffness of the subsoil, whereas there isn't any considerable improvement at higher settlements and low stiffness of the subsoil.

It was observed that there is an increase in load bearing capacity with an increase in geocell layer width (B_g), however, it is always economical to restrict the geocell layer width to 5.

The proposed design charts could be used for designing geocell reinforced strip footing.

The lower value of C induces the confinement effect or stress-dependent behavior and as it increases or tends to infinity it behaves similar to the nonlinear stress independent model. Hence, an appropriate value of C has to be chosen based on the initial stresses.

The improvement that is brought to soft subsoil is significant with the introduction of geocell reinforcement and the soft soil is able to withstand higher loads.

In summary, the present approach of calculating the improvement factors or loads is a better approach as it accounts for the confining stresses in the geocell from which the geocell reinforced subsoil derives its strength.

Nomenclature

B	Width of footing
C	Compaction Coefficient
G_g	Shear modulus of geocell mattress
H	Height of geocell mattress/shear layer
I_f	Improvement factor
k_s	Modulus of subgrade reaction
n	Janbu's Parameter
q_u	Ultimate bearing pressure of unreinforced bed
Q^*	Normalized load (Non-dim)
R_g	Shear layer width ratio (Non-dim)
T	Shear stress
w	Settlement of shear layer from the edge of the footing (m)
W	Normalized settlement
W_0	Normalized footing settlement
X	Distance from center of the footing (m)
X	Normalized distance from center of the footing,
α^2	($ks.B^2/GgH$), inverse of normalized shear stiffness of the geocell reinforced granular layer,
μ	($k_s.B/q_u$), inverse of normalized ultimate bearing capacity of unreinforced soft soil
σ_0	Initial stress
$\Delta\sigma$	Incremental stress
τ	Shear stress

6. REFERENCES

Bathurst R. J. and Jerrett, P. M (1989). "Large-Scale tests of geo-composite mattresses over peat sub grades". Transportation Research Record 1188, Transportation Research Board, Washington, DC, pp. 28 – 36.

Cowland, J.W. and Wong, S. C. K (1993). "Performance of a road embankment on soft clay supported on a geocell mattress foundation". Geotextiles and Geomembranes, 12, pp. 687-705.

Crank, J. and Nicolson, P (1947). "A practical method for numerical evaluation of solutions of partial differential equations of the heat conduction type". Proc. Camb. Phil. Soc., 43 (1), pp. 50–67.

Deb, K., Basudhar, P. K. and Chandra, S (2007). "Generalized Model for Geosynthetic-Reinforced Granular Fill-Soft Soil with Stone Columns". International. Journal of Geomechanics, 7, pp. 266-276.

Faby Mole, P. A, Sireesh, S and Madhav, M. R. (2015), "Numerical Modeling of Strip Footing on Geocell Reinforced Beds", Proceedings of ICE, Ground Improvement, 168, No.3, pp. 194-205.

Janbu, N. (1963). "Soil compressibility as determined by oedometer and triaxial tests," European Conference on Soil Mechanics and Foundation Engineering, Wiesbaden 1, 19-2; 2, 83-87.

Koerner R.M. Designing with geosynthetics, Prentice Hall, Englewood Cliffs, (1990), New Jersey.

Kondner, R. L (1963). "Hyperbolic stress-strain response: cohesive soils". Journal of Soil Mechcanics and Foundation. Division, 89(1), pp. 115–14.

Madhav, M. R. and Poorooshasb, H. B (1988). "A new model for geosynthetic reinforced soil". Computers and Geotechnics, 6, pp. 277-290.

Madhav, M. R. and Poorooshasb, H. B (1989). "Modified Pasternak model for reinforced soil". International Journal of Mathematical and Computer Modelling, 12, pp. 1505-1509.

Moghaddas, S. N. T. and Dawson, A. R. (2010). "Comparison of bearing capacity of a strip footing on sand with geocell and with planar forms of geotextile reinforcement", Geotextiles and Geomembranes, 28, pp. 72–84.

Pasternak, P.L (1954). On a new method of analysis of an elastic foundation by means of two foundation constants (In Russian).

Shukla, SK. Chandra S (1994). "A generalized mechanical model for geosynthetic-reinforced foundation soil". Geotextiles and Geomembranes, 13, pp. 813–82